On the Linearity of External Forcing Response in Solar Geoengineering Experiments

Virgin John G.[1] and Fletcher Christopher G.[1]

[1]University of Waterloo

November 16, 2022

Abstract

To assess impacts of solar geoengineering, the GeoMIP G1 experiment forces Earth System Models with prescribed reductions in solar radiation to balance increases in atmospheric CO_2. One key source of uncertainty is the magnitude of solar constant reduction required to offset a CO_2 quadrupling. Here, we decompose the G1 experiment in the Community Earth System Model with solar only and CO_2 only forcing experiments to quantify single forcing rapid radiative adjustments. We find that radiative adjustments to both single forcings have a net positive effect on top of atmosphere energy balance such that they both increase the net G1 forcing. Stratospheric temperature and shortwave cloud adjustments are the main sources of positive adjustment in both Solar and CO_2 scenarios. We also show that net G1 radiative adjustment cannot be represented linearly with CO2 and solar forcing adjustments, which is primarily traced to further reductions in boundary layer clouds.

On the Linearity of External Forcing Response in Solar Geoengineering Experiments

J. G. Virgin[1], **C. G. Fletcher**[1]

[1]Department of Geography and Environmental Management, University of Waterloo, Waterloo, Ontario, Canada

Key Points:

- The solar constant reduction to balance a CO_2 quadrupling is dependent on radiative adjustments distinct to both solar and CO_2 forcing
- Radiative adjustments as a response to solar and CO_2 forcing cannot be linearly separated using single forcing experiments
- Non-linear adjustments to combined forcings are non-negligible in the net adjustment value in G1 and can primarily be traced to shortwave cloud response

Corresponding author: John Virgin, jgvirgin@uwaterloo.ca

Abstract

To assess impacts of solar geoengineering, the GeoMIP G1 experiment forces Earth System Models with prescribed reductions in solar radiation to balance increases in atmospheric CO_2. One key source of uncertainty is the magnitude of solar constant reduction required to offset a CO_2 quadrupling. Here, we decompose the G1 experiment in the Community Earth System Model with solar only and CO_2 only forcing experiments to quantify single forcing rapid radiative adjustments. We find that radiative adjustments to both single forcings have a net positive effect on top of atmosphere energy balance such that they both increase the net G1 forcing. Stratospheric temperature and shortwave cloud adjustments are the main sources of positive adjustment in both Solar and CO_2 scenarios. We also show that net G1 radiative adjustment cannot be represented linearly with CO_2 and solar forcing adjustments, which is primarily traced to further reductions in boundary layer clouds.

Plain Language Summary

Solar geoengineering refers to the modification of incoming sunlight upon the earth as a means to offset warming from greenhouse gases. Studies using climate models investigate solar geoengineering in an idealized framework by directly tuning the amount of incoming sunlight within a model. The amount of adjusting necessary to achieve energy balance from a given increase in carbon dioxide varies widely from model to model. Here, we run a series of idealized experiments using a state of the art climate model where CO_2 is increased and sunlight is decreased in order to investigate the rapid climate responses to both forcings applied one at a time. We find that rapid climate responses to both reduced sunlight and increased CO_2 are distinct and feed back on on another when forcings are applied together. Furthermore, we find such rapid responses to be the main factor in determining the amount of sunlight reduction needed to balance increased CO_2.

1 Introduction

Solar radiation modification, or solar geoengineering, refers to the deliberate modification of sunlight incident upon the earth as a means of countering anthropogenic climate change. While early studies used simple models to explore the role of solar radiation as an external forcing on the climate system (Wetherald & Manabe, 1975; Hansen et al., 1997), solar geoengineering as a potential mitigating strategy against greenhouse gas induced warming is a theoretical but nascent field of research (Crutzen, 2006; Wigley, 2006; Robock et al., 2009). Coordinated efforts to research geoengineering using Earth System Models (ESMs) began with the Geoengineering Model Inter-comparison Project (GeoMIP) (Kravitz et al., 2011a, 2013a, 2013b, 2015). Initially, core GeoMIP experiment design included of idealized climates where the solar constant was adjusted within a given ESM to offset either instantaneous or time-evolving increases in CO_2. As GeoMIP has evolved over the past decade, more complex experiment designs, such as injections of sulphur dioxide into the stratosphere at the equator to create an aerosol layer analogous to that of a volcanic eruption, have emerged to transition towards more realizable approaches. Application-based experiments such as targeted regional stratospheric aerosol injections (Tilmes et al., 2018), marine cloud albedo enhancement via boundary layer sea salt injections (Latham, 1990; Alterskjær et al., 2012; Niemeier et al., 2013; Kravitz et al., 2013b), calcite aerosol injections (Keith et al., 2016), and cirrus cloud seeding to increase outgoing longwave radiation (Mitchell & Finnegan, 2009) have all been proposed.

Despite the growing breadth of solar geoengineering experiment designs, idealized experiments using direct solar constant tuning have persisted in GeoMIP due to their insights into geoengineered climates and ease of implementation. From both a modeling and implementation standpoint, one element of uncertainty in idealized geoengineer-

ing experiments is the amount of solar constant reduction required to offset a given increase in CO_2. In the GeoMIP G1 experiment, where the solar constant is reduced to balance an abrupt quadrupling of CO_2, the reduction amount varies from model to model between 3.5-5% (Kravitz et al., 2013a, 2021). For modeling groups, determining the necessary reduction is typically circumvented using a brute force approach, where a heuristic equation is used to calculate the globally averaged solar constant reduction needed to offset the radiative forcing from an abrupt quadrupling of CO_2 in order to create an initial guess value. Then, successive simulations with tuned solar constant values are used to achieve energy budget closure (Kravitz et al., 2011b). The solar constant offset model spread has been primarily attributed to rapid adjustments in the climate system as a response to both CO_2 increases and solar constant reductions (Russotto & Ackerman, 2018). Rapid responses in temperature, moisture, and clouds induce radiative perturbations alongside the direct Instantaneous Radiative Forcing (IRF) of the agent itself. which taken together determine the Effective Radiative Forcing (ERF) (Sherwood et al., 2015).

Despite previous work exploring rapid adjustments as a response to external agents, their role in idealized geoengineering scenarios— which involve multiple forcings on the climate system— remain unclear. Here, we decompose the rapid adjustments from both CO_2 and solar forcing in the G1 experiment using a series of single forcing experiments with the Community Earth System Model (CESM). We show that the solar constant offset required is not easily predicted using the heuristic equation from GeoMIP due to adjustments as a response of reducing the solar constant, as well as those that arise non linearly from introducing both CO_2 and solar forcing at the same time. Lastly, we briefly explore the underlying physical response to the non linear adjustment contribution.

2 Methods

2.1 Community Earth System Model

We employ CESM version 1.2.2 in its atmosphere & land only (or "F") component set (Hurrell et al., 2013). Specifically, the component set employed here consists of the Community Atmosphere Model (version 4, CAM4) with 26 vertical levels and 4° x 5° horizontal resolution, the Community Land Model version 4 (CLM4), and prescribed pre-industrial ocean and sea ice climatologies. We configure CAM4 at its 4° x 5° horizontal resolution given our analysis is focused on global and zonal mean quantities, as well as for its computational efficiency. CAM4 is configured with the Cloud Object Simulator Package (COSP, Bodas-Salcedo et al. (2011)) enabled, which includes cloud diagnostics consistent with the International Satellite Cloud Climatology Project (ISCCP) (Klein & Jakob, 1999; Schiffer & Rossow, 1983). The ISCCP diagnostics include cloud fraction as a function of a on a 7 by 7 matrix of cloud top pressure and optical depth, which can be used with cloud radiative kernels to calculate the radiative perturbation associated with cloud responses are various heights and optical depths (Zelinka et al., 2012).

All experiments follow the Radiative Forcing Model Inter-Comparison Project (RFMIP) protocol (Pincus et al., 2016). Simulations are run for 30 years using a repeating annual cycle of pre-industrial sea ice and sea surface climatologies as boundary conditions. All experiments with external forcings are compared to a control simulation where CO_2 and the solar constant are kept at their default pre-industrial values (Table 1). Following RFMIP methodology allows for direct calculation of the ERF for each experiment. This offers a distinct advantage relative to the so-called "Gregory" method, which relies on using linear regression on coupled model output in order to extrapolate the ERF (Gregory et al., 2004), and is therefore subject to drawbacks of assuming linearity in the climate response to changes global mean surface temperature (Knutti et al., 2017). Furthermore, the Gregory approach is significantly more computationally expensive given it requires centuries of coupled atmosphere-ocean model simulation.

We follow the GeoMIP G1 protocol to estimate the necessary solar constant reduction needed to offset increased CO_2 (Kravitz et al., 2011b). The G1 experiment design targets TOA energy balance as a metric of effectiveness. Specifically, we calculate the solar constant reduction using the following equation:

$$ERF_{CO_2} = \frac{\Delta S_0 \pi r^2}{4\pi r^2}(1-\alpha), \tag{1}$$

where ERF_{CO_2} is the ERF from a quadrupling of CO_2, r is the radius of the Earth, α is the planetary albedo (calculated using the abrupt-4xCO_2 simulation), and ΔS_0 is the solar constant reduction. For G1 simulations submitted to GeoMIP, this equation is to be satisfied for coupled simulations ran for 50 years. While this approach was adhered to for the majority of GeoMIP G1 simulations, some models targeted global mean surface temperature as opposed to energy balance.

First, we run an abrupt-4xCO_2 experiment (herein referred to as 4xCO_2) and take the difference between 30 year global mean net top of atmosphere radiation relative to the control experiment to quantify the ERF_{CO_2} (Hansen et al., 2005). We use the same prescribed value of ΔS_0 as calculated via Equation 1 for both solar forcing only (herein referred to as SOLAR) and G1 experiments, where in G1 an abrupt quadrupling of CO_2 and solar constant reduction are applied at the same time. To estimate the linearity of the response, we also compute the sum of the outputs from the SOLAR and 4xCO_2 single-forcing experiments, and refer to the resulting output as the G1L experiment.

Experiment	CO_2 (ppm)	Solar Constant (W m^{-2})	Note
Control	284.7	1360.89	Baseline
4xCO_2	1138.8	1360.89	single forcing
SOLAR	284.7	1317.19	single forcing
G1	1138.8	1317.19	combined forcings
G1L	1138.8	1317.19	SOLAR + 4xCO_2 output

Table 1. Experiments performed for this study with their respective settings for CO_2 volume mixing ratio and solar constant values.

2.2 Quantifying Radiative Perturbations

We estimate the change in TOA energy balance in each experiment using the following equation:

$$ERF = IRF + \sum_{x}^{n} \frac{\partial R}{\partial x} dx \tag{2}$$

where ERF is the Effective Radiative Forcing for a given climate forcing (4xCO_2, SOLAR), IRF is the Instantaneous Radiative Forcing, and the summation term is the sum of all radiative adjustments from responses in surface albedo, temperature, water vapor, and clouds. We clarify the term "adjustments" as opposed to "feedbacks" given the RFMIP experiment design where all SSTs and sea ice are prescribed. The partial term ($\frac{\partial R}{\partial x}$) represents the radiative sensitivities of a given state variable (x), and dx represents the climate response in x due to the external forcing of SOLAR, 4xCO_2, and G1 relative to the Control simulation.

We quantify the ERF directly from model output as the difference of 30 year, annual mean net TOA radiation in forcing experiments relative to the Control experiment. Each non-cloud radiative adjustment is quantified using radiative kernels (Shell et al., 2008). We use the radiative kernels from Shell et al. (2008) specifically as they were computed using radiative transfer code (CAMRT (Collins et al., 2004)) most similar as to the version of CESM used for this study. All radiative kernels are interpolated to 4° x 5° horizontal resolution and all climate responses are interpolated down to 17 standard CMIP5 pressure levels (where applicable) before applying the radiative kernels. We quantify cloud adjustments using the COSP output from CESM and cloud radiative kernels designed for use with GCMs (Zelinka et al., 2012, 2013, 2016). Using the cloud kernel method, cloud radiative adjustments can be decomposed into contributions from both boundary layer ($\geq$ 680 hPa) and free troposphere ($<$ 680 hPa) clouds in both the longwave and shortwave[1]. Lastly, we quantify the IRF as the residual of the ERF and all radiative adjustments via rearranging the terms in Equation 2. Under this framework where all radiative adjustments and the ERF are explicitly quantified, we assume that any error due to non-linearities in the energy budget decomposition (Equation 1) is small enough to consider negligible and thus included in the IRF term.

3 Results

3.1 Energy Budget Residual in G1

We begin by showing the TOA energy budget response (i.e. the ERF) for each experiment in our study. The global mean ERF for 4xCO_2 is 7.21 W m^{-2} (Figure 1a). Using this value in equation 1 predicts ΔS_0 of 43.70 W m^{-2} would be required to offset the ERF_{CO_2}. However, the ERF for SOLAR is -6.46 W m^{-2}, indicating that the S_0 offset is insufficient to fully balance ERF_{CO_2}, and this is confirmed by the residual ERF of 0.93 W m^{-2} in the G1 experiment. While this residual is relatively small in the context of the global planetary energy budget, GeoMIP protocol requires ESMs to be within 0.1 W m^{-2} of energy balance (Kravitz et al., 2011a). That Equation 1 produces a positive residual in ERF (i.e. it underestimates ΔS_0 required to balance 4xCO2 forcing) is well-documented (Russotto & Ackerman, 2018), but to our knowledge has not been adequately explained by previous studies.

The remainder of this section presents the physical evidence for why this imbalance exists. The first piece of evidence comes from the meridional structure of ERF in response to 4xCO_2 and SOLAR forcing. For 4xCO_2, ERF peaks in the tropics and decreases toward the poles (Figure 1b), in line with previous studies linking its meridional structure to the Planck response of warmer emission temperatures (Zhang & Huang, 2014). The SOLAR ERF is strongest (more negative) over the tropics and weakest (more positive) near the poles, which arises from the tropics receiving the largest fraction of insolation globally and thus the largest fractional decrease as a result of ΔS_0. In G1 the ERF is near zero throughout the tropics, indicating almost perfect cancellation there, but there is a residual in extratropical regions in both hemispheres (Figure 1b). Subsampling the response into 3 decadal means shows that both the global mean ERF and its meridional structure is qualitatively similar for all three experiments.

Given that ERF takes into account all radiative adjustments from temperature, surface albedo, water vapour, and clouds, it is insufficient as a stand alone metric to assess linearity between single versus combined forcing experiments. For SOLAR and 4xCO_2 specifically, differences in both sign and magnitude of radiative adjustments have been linked to residual positive forcing in GeoMIP G1 experiments (Russotto & Ackerman,

[1] See Zelinka et al. (2016) supplementary information for more methodological details

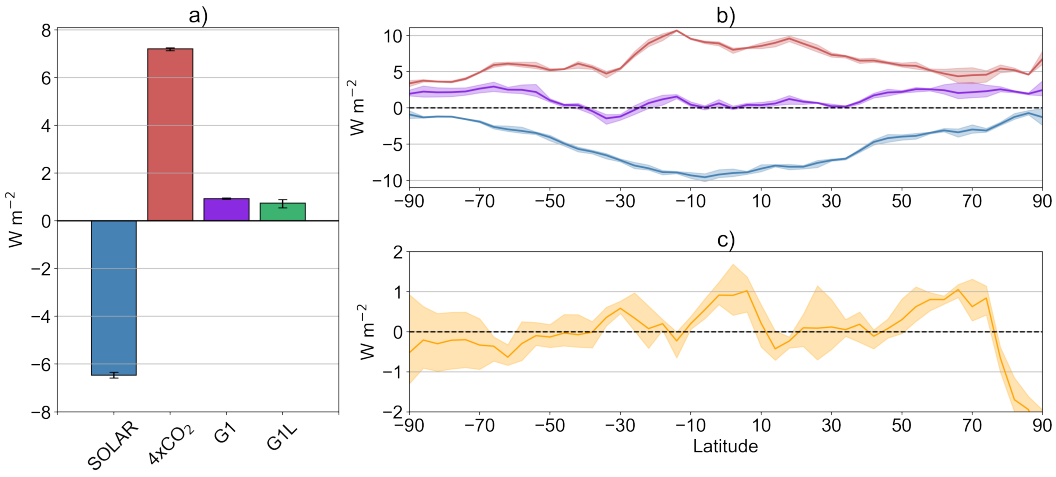

Figure 1. a) Global mean ERF values for SOLAR, 4xCO$_2$, G1, and G1L experiments. Error bars are calculated via subsampling the response into 3 decadal mean intervals (years 1-10, 11-20, and 21-30) and taking the difference between the maximum and minimum intervals. b) The corresponding Zonal mean ERF. c) Zonal mean residual ERF between G1-G1L experiments. For subplots b and c, the shaded regions are calculated as in subplot a.

2018). To understand what drives the nonlinearity in the response, we now present the decomposition of ERF decomposed into the IRF and its individual radiative adjustments.

The net radiative adjustment in G1 is 3.26 W m^{-2}, which is explained primarily by positive adjustments from stratospheric temperature and both boundary layer and free troposphere clouds in the SW, and partially offset by a negative Planck adjustment (Figure 2a). The net G1 adjustment illustrates the importance of quantifying rapid responses here with respect to achieving energy balance, as the G1 ERF is only slightly positive (0.93 W m^{-2}, Figure 1a) and would thus be substantially more negative without rapid adjustments. By construction, the Planck adjustment entirely explained by land surface temperature changes because SSTs and sea ice boundary conditions remain fixed. The land surface warms in G1 and 4xCO$_2$, and cools in SOLAR (Figure S1). While other radiative adjustments are non-zero, the breakdown from G1 into 4xCO$_2$ and SOLAR shows that in many cases this is due to adjustments offsetting one another in terms of experiment. For example, the surface albedo adjustment is weakly positive (negative) for 4xCO$_2$ (SOLAR), which is linked to land surface warming (cooling) and subsequent reductions in snow cover (Kuang & Yung, 2000). In terms of magnitude, the biggest contributions to G1 are from certain adjustments that are positive in both 4xCO$_2$ and SOLAR. The stratospheric temperature adjustment is positive due to radiative cooling in both single forcing experiments, a result that has been consistently observed across modelling studies (Wang & Huang, 2020; Chung & Soden, 2015; Hansen et al., 2005; Manabe & Wetherald, 1975). The SW cloud adjustments are partitioned into boundary layer and free troposphere components, both of which are positive for 4xCO$_2$ and SOLAR scenarios, indicative of widespread reduction in cloud amount and/or optical depth throughout the troposphere. Conversely, LW cloud adjustments are near zero across all experiments and both cloud top distinctions. The contrast between longwave and shortwave cloud adjustments is linked to experiment workflow here, where SW heating from cloud fraction reduction is primarily linked to fast responses after a forcing agent has been introduced and LW heating is mostly surface temperature mediated (i.e. a feedback) (Zelinka et al., 2013). Given our experiments hold SSTs fixed, the longwave effect of cloud adjustments is near zero.

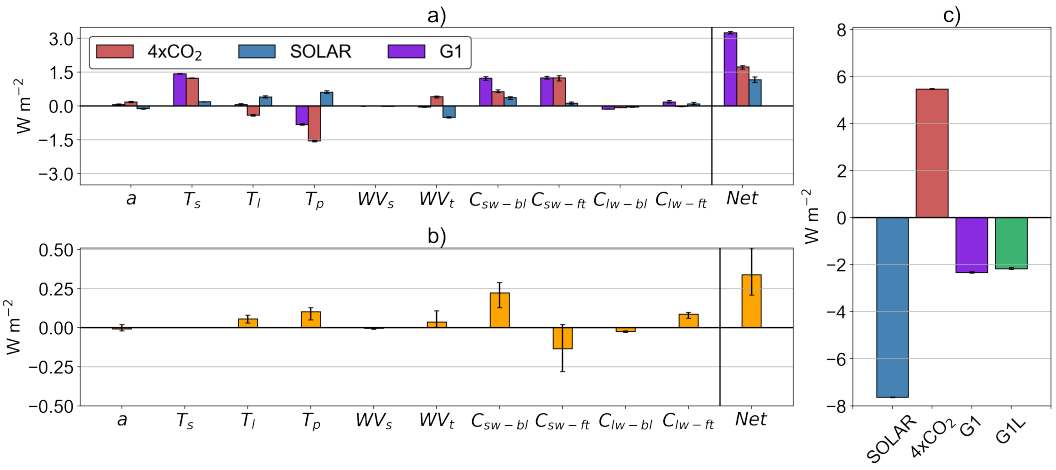

Figure 2. Global, annual mean radiative adjustments for a) CO_2, SOLAR, and G1 experiments and b) Residual error between G1 and G1L experiments. From left to right, adjustments are listed as surface albedo (a), stratospheric temperature (T_s), lapse rate $T_{(l)}$, Planck (T_p), stratospheric water vapour (WV_s), tropospheric water vapour (Wv_t), shortwave boundary layer cloud ($C_{sw\text{-}bl}$), shortwave free troposphere cloud ($C_{sw\text{-}ft}$), longwave boundary layer cloud ($C_{lw\text{-}bl}$), longwave free troposphere cloud ($C_{lw\text{-}ft}$), and the total radiative adjustment value (net). c) Global mean IRF for all four experiments. Error bars for all three subplots are calculated in the same way as described in Figure 1.

Positive adjustments in both 4xCO_2 and SOLAR experiments highlight why Equation 1 often under predicts the ΔS_0 offset to balance increased CO_2. Adjustments positively affect the IRF for 4xCO_2 and SOLAR, but not in equal amounts. Equation 1 only considers adjustments from CO_2, not adjustments for the solar constant reduction or potential non-linear interactions between the combined forcings. This result is also supported by the global mean IRF for both 4xCO_2 and SOLAR. In G1, the negative instantaneous forcing (-2.33 W m^{-2}) is the result of all adjustments from 4xCO_2 (+1.74 W m^{-2}, Figure 2a) being factored into Equation 1, which necessitates a greater reduction in the solar constant and thus a more negative SOLAR instantaneous radiative forcing (Figure 2c). Indeed, if one were to use the IRF from 4xCO_2 in equation 1, ΔS_0 would be 33.15 W m^{-2} as opposed to 43.70 W m^{-2}. Next, we quantify and decompose the radiative adjustments associated with non-linear responses to both 4xCO_2 and SOLAR forcings.

3.2 Non-linear Responses to Combined Forcings

Using G1L provides a useful baseline to quantify non-linearities in G1. Any residual in the energy budget between the two experiments is, by construction, a product of feedbacks in the climate response that cause radiative adjustments and further perturb the energy budget in G1. There is a non-negligible residual between the global mean ERF of G1 and G1L experiments (G1 is +0.19 W m^{-2} higher than G1L), which indicates that non-linear responses contribute to the positive adjustments from both SOLAR and 4xCO_2 rather than offset them (Figure 1a). Spatially, the energy budget residual is largest between the two experiments in the Arctic region, where G1 has a weaker ERF by as much as 2 W m^{-2} (Figure 1c). However, the global mean residual is positive, with distinct peaks in the equatorial region and northern hemisphere extratropics.

The magnitude and sign of most adjustments is approximated by the linear sum of 4xCO_2 and SOLAR experiments (Figure 2b). The largest residuals come from the SW

boundary layer cloud adjustment (+0.22 W m^{-2}), the SW free troposphere cloud adjustment (-0.13 W m^{-2}), and the Planck adjustment (+0.10 W m^{-2}). The G1 net residual value is 0.34 W m^{-2}, or 10.45% of the net radiative adjustment value in G1. The SW free troposphere cloud adjustment residual exhibits substantial spread depending on which period of the response is considered, which results in a maximum net adjustment residual as high as 0.51 W m^{-2}. This net positive residual and its contributing components are indicative of non-linear interactions between cloud and thermodynamic responses in G1 that act collectively to further reduce cloud amount and/or optical depth in addition to the linearly additive response in G1L.

In G1, total cloud radiative adjustments are largely dominated by 4xCO_2, with responses from SOLAR being limited to boundary layer clouds (Figure 2a). Figure 3a shows the global mean G1 ISCCP simulator cloud fraction response consistent with the radiative adjustments calculated in the previous section. G1 exhibits reductions in optically thick clouds throughout the free troposphere from 60°S - 60°N (Figure 3a and c). Reduced cloud fraction has a positive radiative effect in the SW as less radiation is reflected back to the TOA, causing a positive adjustment for both boundary layer and free troposphere clouds (Figure 2a). Cloud fraction increases near the tropopause, but the LW radiative effect is small due to such increases being confined to optically thin clouds (Figure 2a, Figure 3a). Other increases in free troposphere clouds are confined to the poles in G1 (not shown), so they exhibit little influence on global mean radiative adjustments.

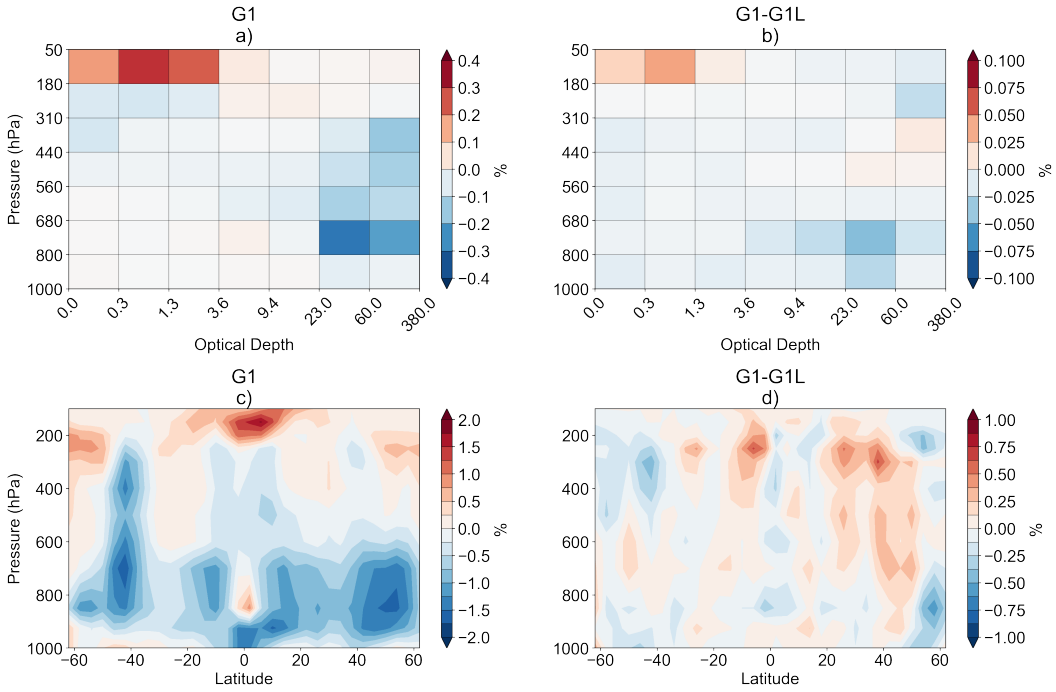

Figure 3. a) Global, annual mean ISCCP simulator cloud fraction response (30 year means) for G1. b) Residual ISCCP simulator cloud fraction response between G1-G1L. c & d) Same as a & c but for zonal mean total cloud fraction on standard CMIP5 pressure levels.

The largest nonlinear contribution to the global mean is from optically thick boundary layer clouds (Figure 3b). Negative residuals in the lower troposphere below 680hPa illustrate further reduction in cloudiness in G1 and provide a clear explanation for the residual in SW low cloud adjustment (Figure 2b, Figure 3d). Conversely, the largest positive residuals are in the upper troposphere, indicating a nonlinear amplification of op-

tically thin clouds in G1 relative to G1L. The small positive residuals in optically thick bins from 310-560 hPa show less of a cloud fraction reduction in G1. However, there is substantial spread in the corresponding SW free troposhere radiative adjustment depending on which subsampled time frame is used as the response (i.e. years 1-10 or 21-30, Figure 2b). The magnitude and sign of cloud adjustments to external forcings persist as a dominant source of ERF uncertainty across ESMs (C. J. Smith et al., 2020). While these results are from a single model, they qualitatively agree with results assessing multi-model ensemble cloud adjustments as a response to increased CO_2 (Kamae & Watanabe, 2012). Our results also show that the free troposphere cloud response in G1 is dominated by the CO_2 forcing as opposed to solar forcing (Figure 2a). As LW heating from the CO_2 IRF warms and dries the lower free troposphere, relatively drier air is mixed downward from aloft to decrease optically thick boundary layer clouds in subsiding regions (Figure S2) (Kamae & Watanabe, 2012). Under solar forcing, the troposphere cools while the SSTs remain fixed, reducing inversion strength in those same subsiding regions and further decreasing cloud fraction. While the radiative magnitude of this effect is smaller in SOLAR (Figure 2a), the first order dependence on inversion strength is well documented as a controlling factor on low latitude boundary layer clouds (Klein et al., 2017).

4 Discussion and Conclusions

In this study, we have decomposed the top of atmosphere energy budget in a series of fixed-SST, single and multi-forcing experiments using CESM to clarify the role of rapid adjustments in an idealized geoengineering scenario. Rapid adjustments act to increase the IRF for both 4xCO_2 and SOLAR forcing. In the context of the G1 experiment with 4xCO_2 and SOLAR forcing combined, this dampens the desired effect on TOA energy balance of reducing the solar constant, which necessitates overshooting the amount of reduction predicted by Equation 1. A decomposition of radiative adjustments to each external forcing within G1 reveals a significant non-linear effect that amplifies the net positive adjustment– primarily by reducing boundary layer cloud amount. A physical driver for such a non-linear response is not immediately clear. Decomposing the low cloud response in G1 and G1L into contributions from cloud controlling factors may offer some insight (Scott et al., 2020; Klein et al., 2017; Qu et al., 2015), but such work is beyond the scope of this study.

From a modeling perspective, our results illustrate the difficulty in achieving energy budget closure at the top of atmosphere for G1 via a trial and error approach. Even if one were to run a solar forcing only experiment to quantify the net radiative adjustment as done here, which could then be factored back into Equation 1, it would likely be ineffective as the net adjustment would vary as a function of the offset itself, which would then produce a secondary non-linear effect when both forcings are combined within a G1 experiment. Moreover, our results presented here are from a single ESM, and the non-linear adjustment contribution in G1 experiments likely varies from model to model to a similar degree as for other external forcings (C. Smith et al., 2018). More recent advancements have taken a different approach, where geoengineering methodologies are designed to meet a particular objective (e.g. preserving the equator-to-pole surface temperature gradient) (Kravitz et al., 2016). Such an approach is in contrast to the conventional approach explored here, where the methodology is applied and its effectiveness evaluated afterwards.

An intuitive next step would be to assess the role of rapid adjustments in transient or plausible solar geoengineering scenarios. Solar dimming experiments do not wholly capture modeled responses from aerosol injections, particularly with regards to atmospheric chemistry and dynamics (Visioni et al., 2021a). Results from GeoMIP6 transient scenarios show that fully coupled ESMs exhibit similar globally averaged surface responses regardless of whether or not external forcings are applied smoothly or as a once per decade step function (Visioni et al., 2021b). Nevertheless, decomposing rapid adjustments to

individual forcings in transient geoengineering scenarios could reveal regional climate responses and underlying non-linear physical drivers as shown here.

Complications for modeling centres notwithstanding, these results exemplify the need for further research on rapid adjustments in geoengineering scenarios, particularly for ones with real world applicability as it will be an integral component in quantifying both geoengineering effectiveness (in terms of energy budget or surface temperature based objectives) and near term impacts (in terms of rapid climate response).

Open Research

All post-processing, analysis, and plotting scripts for this study can be found on J.G. Virgin's Github page (https://github.com/JohnVirgin). Experiment output for all 3 CESM experiments ran for this study are publicly available and stored on the Univerisity of Waterloo Dataverse (https://doi.org/10.5683/SP3/2UVOPO). Source code for CESM is publicly available (https://www.cesm.ucar.edu/models/cesm2/release_download.html).

Acknowledgments
The authors thank Karen Smith and Jason N.S. Cole for their thoughtful comments which helped strengthen the manuscript. We also acknowledge the support of the Natural Sciences and Engineering Research Council of Canada (NSERC). All data produced for this study is with the open source Community Earth System Model (CESM).

References

Alterskjær, K., Kristjánsson, J., & Seland, Ø. (2012). Sensitivity to deliberate sea salt seeding of marine clouds–observations and model simulations. *Atmospheric Chemistry and Physics*, *12*(5), 2795–2807.

Bodas-Salcedo, A., Webb, M., Bony, S., Chepfer, H., Dufresne, J.-L., Klein, S., ... others (2011). Cosp: Satellite simulation software for model assessment. *Bulletin of the American Meteorological Society*, *92*(8), 1023–1043.

Chung, E.-S., & Soden, B. J. (2015). An assessment of direct radiative forcing, radiative adjustments, and radiative feedbacks in coupled ocean–atmosphere models. *Journal of Climate*, *28*(10), 4152–4170.

Collins, W. D., Rasch, P. J., Boville, B. A., Hack, J. J., McCaa, J. R., Williamson, D. L., ... others (2004). Description of the ncar community atmosphere model (cam 3.0). *NCAR Tech. Note NCAR/TN-464+ STR*, *226*, 1326–1334.

Crutzen, P. J. (2006). Albedo enhancement by stratospheric sulfur injections: A contribution to resolve a policy dilemma? *Climatic change*, *77*(3-4), 211.

Gregory, J., Ingram, W., Palmer, M., Jones, G., Stott, P., Thorpe, R., ... Williams, K. (2004). A new method for diagnosing radiative forcing and climate sensitivity. *Geophysical research letters*, *31*(3).

Hansen, J., Sato, M., & Ruedy, R. (1997). Radiative forcing and climate response. *Journal of Geophysical Research: Atmospheres*, *102*(D6), 6831–6864.

Hansen, J., Sato, M., Ruedy, R., Nazarenko, L., Lacis, A., Schmidt, G., ... others (2005). Efficacy of climate forcings. *Journal of geophysical research: atmospheres*, *110*(D18).

Hurrell, J. W., Holland, M. M., Gent, P. R., Ghan, S., Kay, J. E., Kushner, P. J., ... others (2013). The community earth system model: a framework for collaborative research. *Bulletin of the American Meteorological Society*, *94*(9), 1339–1360.

Kamae, Y., & Watanabe, M. (2012). On the robustness of tropospheric adjustment in cmip5 models. *Geophysical Research Letters*, *39*(23).

Keith, D. W., Weisenstein, D. K., Dykema, J. A., & Keutsch, F. N. (2016). Stratospheric solar geoengineering without ozone loss. *Proceedings of the National*

academy of Sciences, *113*(52), 14910–14914.

Klein, S. A., Hall, A., Norris, J. R., & Pincus, R. (2017). Low-cloud feedbacks from cloud-controlling factors: A review. *Shallow clouds, water vapor, circulation, and climate sensitivity*, 135–157.

Klein, S. A., & Jakob, C. (1999). Validation and sensitivities of frontal clouds simulated by the ecmwf model. *Monthly weather review*, *127*(10), 2514–2531.

Knutti, R., Rugenstein, M. A., & Hegerl, G. C. (2017). Beyond equilibrium climate sensitivity. *Nature Geoscience*, *10*(10), 727–736.

Kravitz, B., Caldeira, K., Boucher, O., Robock, A., Rasch, P. J., Alterskjær, K., ... others (2013a). Climate model response from the geoengineering model intercomparison project (geomip). *Journal of Geophysical Research: Atmospheres*, *118*(15), 8320–8332.

Kravitz, B., Forster, P. M., Jones, A., Robock, A., Alterskjær, K., Boucher, O., ... others (2013b). Sea spray geoengineering experiments in the geoengineering model intercomparison project (geomip): Experimental design and preliminary results. *Journal of Geophysical Research: Atmospheres*, *118*(19), 11–175.

Kravitz, B., MacMartin, D. G., Visioni, D., Boucher, O., Cole, J. N., Haywood, J., ... others (2021). Comparing different generations of idealized solar geoengineering simulations in the geoengineering model intercomparison project (geomip). *Atmospheric Chemistry and Physics*, *21*(6), 4231–4247.

Kravitz, B., MacMartin, D. G., Wang, H., & Rasch, P. J. (2016). Geoengineering as a design problem. *Earth System Dynamics*, *7*(2), 469–497.

Kravitz, B., Robock, A., Boucher, O., Schmidt, H., Taylor, K., Stenchikov, G., & Michael, S. (2011b). Specifications for geomip experiments g1 through g4. *Ben Kravitz*.

Kravitz, B., Robock, A., Boucher, O., Schmidt, H., Taylor, K. E., Stenchikov, G., & Schulz, M. (2011a). The geoengineering model intercomparison project (geomip). *Atmospheric Science Letters*, *12*(2), 162–167.

Kravitz, B., Robock, A., Tilmes, S., Boucher, O., English, J. M., Irvine, P. J., ... others (2015). The geoengineering model intercomparison project phase 6 (geomip6): Simulation design and preliminary results. *Geoscientific Model Development*, *8*(10), 3379–3392.

Kuang, Z., & Yung, Y. L. (2000). Observed albedo decrease related to the spring snow retreat. *Geophysical research letters*, *27*(9), 1299–1302.

Latham, J. (1990). Control of global warming? *Nature*, *347*(6291), 339–340.

Manabe, S., & Wetherald, R. T. (1975). The effects of doubling the co2 concentration on the climate of a general circulation model. *Journal of Atmospheric Sciences*, *32*(1), 3–15.

Mitchell, D. L., & Finnegan, W. (2009). Modification of cirrus clouds to reduce global warming. *Environmental Research Letters*, *4*(4), 045102.

Niemeier, U., Schmidt, H., Alterskjær, K., & Kristjánsson, J. (2013). Solar irradiance reduction via climate engineering: Impact of different techniques on the energy balance and the hydrological cycle. *Journal of Geophysical Research: Atmospheres*, *118*(21), 11–905.

Pincus, R., Forster, P. M., & Stevens, B. (2016). The radiative forcing model intercomparison project (rfmip): experimental protocol for cmip6. *Geoscientific Model Development*, *9*(9), 3447–3460.

Qu, X., Hall, A., Klein, S. A., & DeAngelis, A. M. (2015). Positive tropical marine low-cloud cover feedback inferred from cloud-controlling factors. *Geophysical Research Letters*, *42*(18), 7767–7775.

Robock, A., Marquardt, A., Kravitz, B., & Stenchikov, G. (2009). Benefits, risks, and costs of stratospheric geoengineering. *Geophysical Research Letters*, *36*(19).

Russotto, R. D., & Ackerman, T. P. (2018). Changes in clouds and thermodynamics under solar geoengineering and implications for required solar reduction. *At-*

mospheric Chemistry and Physics, *18*(16), 11905–11925.

Schiffer, R. A., & Rossow, W. B. (1983). The international satellite cloud climatology project (isccp): The first project of the world climate research programme. *Bulletin of the American Meteorological Society*, *64*(7), 779–784.

Scott, R. C., Myers, T. A., Norris, J. R., Zelinka, M. D., Klein, S. A., Sun, M., & Doelling, D. R. (2020). Observed sensitivity of low-cloud radiative effects to meteorological perturbations over the global oceans. *Journal of Climate*, *33*(18), 7717–7734.

Shell, K. M., Kiehl, J. T., & Shields, C. A. (2008). Using the radiative kernel technique to calculate climate feedbacks in ncar's community atmospheric model. *Journal of Climate*, *21*(10), 2269–2282.

Sherwood, S. C., Bony, S., Boucher, O., Bretherton, C., Forster, P. M., Gregory, J. M., & Stevens, B. (2015). Adjustments in the forcing-feedback framework for understanding climate change. *Bulletin of the American Meteorological Society*, *96*(2), 217–228.

Smith, C., Kramer, R., Myhre, G., Forster, P., Soden, B., Andrews, T., ... others (2018). Understanding rapid adjustments to diverse forcing agents. *Geophysical Research Letters*, *45*(21), 12–023.

Smith, C. J., Kramer, R. J., Myhre, G., Alterskjær, K., Collins, W., Sima, A., ... others (2020). Effective radiative forcing and adjustments in cmip6 models. *Atmospheric Chemistry and Physics*, *20*(16), 9591–9618.

Tilmes, S., Richter, J. H., Kravitz, B., MacMartin, D. G., Mills, M. J., Simpson, I. R., ... others (2018). Cesm1 (waccm) stratospheric aerosol geoengineering large ensemble project. *Bulletin of the American Meteorological Society*, *99*(11), 2361–2371.

Visioni, D., MacMartin, D. G., & Kravitz, B. (2021a). Is turning down the sun a good proxy for stratospheric sulfate geoengineering? *Journal of Geophysical Research: Atmospheres*, *126*(5), e2020JD033952.

Visioni, D., MacMartin, D. G., Kravitz, B., Boucher, O., Jones, A., Lurton, T., ... others (2021b). Identifying the sources of uncertainty in climate model simulations of solar radiation modification with the g6sulfur and g6solar geoengineering model intercomparison project (geomip) simulations. *Atmospheric Chemistry and Physics*, *21*(13), 10039–10063.

Wang, Y., & Huang, Y. (2020). Understanding the atmospheric temperature adjustment to co2 perturbation at the process level. *Journal of Climate*, *33*(3), 787–803.

Wetherald, R. T., & Manabe, S. (1975). The effects of changing the solar constant on the climate of a general circulation model. *Journal of Atmospheric Sciences*, *32*(11), 2044–2059.

Wigley, T. M. (2006). A combined mitigation/geoengineering approach to climate stabilization. *Science*, *314*(5798), 452–454.

Zelinka, M. D., Klein, S. A., & Hartmann, D. L. (2012). Computing and partitioning cloud feedbacks using cloud property histograms. part i: Cloud radiative kernels. *Journal of Climate*, *25*(11), 3715–3735.

Zelinka, M. D., Klein, S. A., Taylor, K. E., Andrews, T., Webb, M. J., Gregory, J. M., & Forster, P. M. (2013). Contributions of different cloud types to feedbacks and rapid adjustments in cmip5. *Journal of Climate*, *26*(14), 5007–5027.

Zelinka, M. D., Zhou, C., & Klein, S. A. (2016). Insights from a refined decomposition of cloud feedbacks. *Geophysical Research Letters*, *43*(17), 9259–9269.

Zhang, M., & Huang, Y. (2014). Radiative forcing of quadrupling co2. *Journal of Climate*, *27*(7), 2496–2508.

Supporting Information for "On the Linearity of External Forcing Response in Solar Geoengineering Experiments"

J. G. Virgin[1], C. G. Fletcher[1]

[1]Department of Geography & Environmental Management, University of Waterloo, Waterloo, Ontario, Canada

Contents of this file

1. Figures S1 to S2

Figures

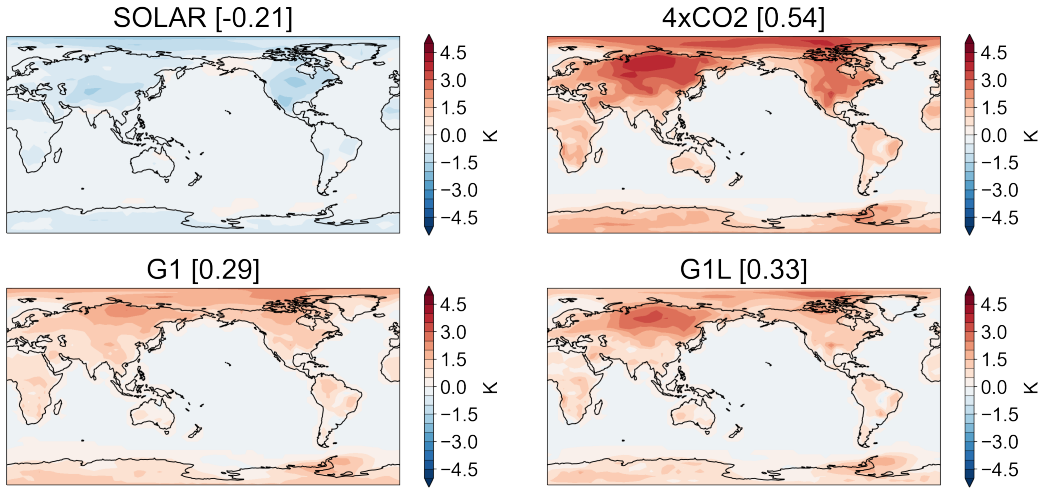

Figure S1. Annual mean surface temperature responses for a) SOLAR, b) $4xCO_2$, c) G1, and d) G1L experiments. values in square brackets are global means.

å

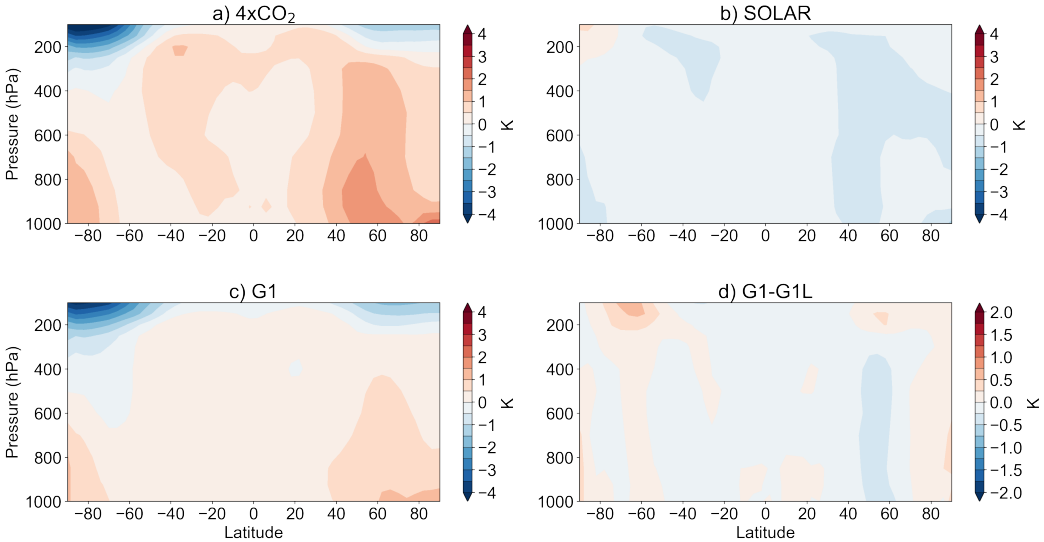

Figure S2. 30 year zonal, annual mean air temperature response for a) $4xCO_2$, b) SOLAR, c) G1, and d) G1-G1L.